The persistence of trip-induced spanwise periodicity in developing turbulent boundary layers

R. Baidya
Dept. Mech. Eng.
The University of Melbourne
Victoria 3010, Australia
baidyar@unimelb.edu.au

C. M. de Silva
Dept. Mech. Eng.
The University of Melbourne
Victoria 3010, Australia
deslivac@unimelb.edu.au

L. Castillo
Dept. Mech. Eng.
Texas Tech University
Lubbock, TX 79409-1021, USA
luciano.castillo@ttu.edu

I. Marusic
Dept. Mech. Eng.
The University of Melbourne
Victoria 3010, Australia
imarusic@unimelb.edu.au

N. Hutchins
Dept. Mech. Eng.
The University of Melbourne
Victoria 3010, Australia
nhu@unimelb.edu.au

Abstract

The present work investigates spanwise periodic modes introduced at the inception point (trip) of a developing turbulent boundary layer. Empirical evidence suggests that these modes can be persistent, and the idea here is to exploit this apparent persistence/amplification of weak lateral variations in turbulent boundary layers, to explore whether the downstream evolution can be substantially modified. Preliminary results, where micro vortex generators are used to introduce the spanwise modes at the trip, indicate the presence of spanwise alternating modes. These modes appear to strengthen after some distance downstream of their introduction for certain configurations (this strengthening can occur almost 350 blade heights downstream of the trip). Further, the spanwise wavelength of the trip seems to play a critical role in determining the downstream development and subsequent evolution of the turbulent boundary layer towards a canonical state. Collectively, these findings suggest that three-dimensionality introduced at the trip may be a viable approach to perturb the evolution of developing turbulent boundary layers over a large streamwise development length.

Introduction

A turbulent boundary layer forming on a flat plate appears to exhibit a lateral instability during its development that can sustain and amplify initially weak spanwise perturbations. For example, persistent lateral variations have been observed within developing turbulent boundary layers, even in carefully fabricated, well-controlled wind tunnel facilities with nominally uniform free-stream conditions (Klebanoff & Tidstrom, 1959; Watmuff, 1998). These modes are thought to arise due to subtle imperfections in the upstream screens used for flow conditioning (Bradshaw, 1965; Furuya *et al.*, 1979; Pook *et al.*, 2016). Townsend (1976, pp. 328-331) demonstrated analytically that small lateral variations in turbulent boundary layers tend to be selectively amplified up to a critical amplitude as the boundary layer develops, with the most amplified or dominant wavelengths tending to be those that are on the order of the boundary layer thickness (δ). In the case of the studies mentioned above, it is thought that these lateral variations may be introduced from weak flow imperfections in the free-stream. However, these spanwise variations could also be introduced or exacerbated by surface roughness (Gong *et al.*, 1996; Mejia-Alvarez & Christensen, 2013; Reynolds *et al.*, 2007).

To investigate this phenomenon, the present work examines the downstream persistence of lateral variations introduced at the inception point (or trip) in a developing zero pressure gradient turbulent boundary layer. In doing so we hope to shed light on the ability of the developing turbulent boundary layer to selectively amplify approximately δ-scaled spanwise variations—as proposed by Townsend (1976)—out of pre-existing heterogeneity (this could be heterogeneity in the free-stream, in the trip, or in the surface stress conditions). A further aim here is to investigate the viability of controlling or perturbing the evolution of the developing turbulent boundary layer through embedded spanwise perturbations.

A number of studies have investigated the evolution of the turbulent boundary layer under different tripping conditions. For example, Schlatter & Örlü (2011), using direct numerical simulations of developing turbulent boundary layers, have shown that relatively minor modifications to the trip parameters can produce non-canonical development up to surprisingly high Reynolds numbers. Marusic *et al.* (2015) demonstrated similar results experimentally, finding non-canonical development to even higher Reynolds numbers (however, in these cases the trip perturbation was rather aggressive). Here, we plan to exploit the ability of a relatively modest spanwise perturbation to excite persistent δ-scaled spanwise modes, to attain both a further reaching and efficient modification to the evolution of a turbulent boundary layer. This idea is largely underpinned by the suggestion of Castillo & Johansson (2002) who noted that upstream conditions could impose a profound influence on the downstream development. Based on these findings they proposed that flow control initiated from upstream manipulations could provide a viable avenue of research for turbulent boundary layer control.

For the preliminary results discussed here, spanwise periodic disturbances are introduced at the trip of a turbulent boundary layer using a series of micro vortex generators (MVGs). By systematically changing the MVG wavelength and mapping how the mean velocity changes with the development distance, we investigate the ability of a turbulent boundary layer to self-sustain certain spanwise periodic modes.

Experimental Set-up

The experiments are performed in the High Reynolds Number Boundary Layer Wind Tunnel (HRNBLWT) at the University of Melbourne (Nickels *et al.*, 2005). Figure 1 shows an overall view of the experimental campaign, which employs both hot-wire anemometry and particle image velocimetry (PIV) measurements. Typically, the boundary layer in the facility is tripped using a strip of 40 grit sand paper (SP40); and this will correspond to our reference case. Spanwise-periodic modes are introduced using a series of MVGs

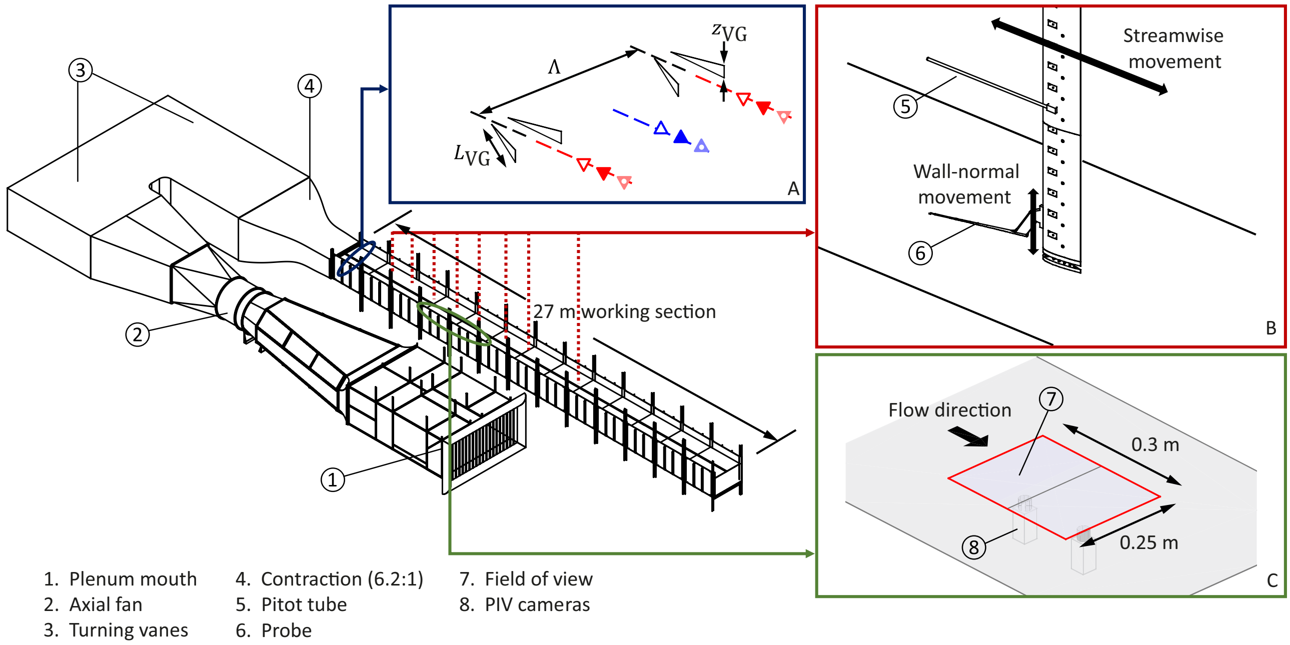

Figure 1: An overview of experimental campaign. The left schematic shows HRNBLWT (adapted from Baars *et al.*, 2016), while the vertical dotted lines indicate the measurement stations. The insets A-C illustrate the micro vortex generators (MVG), hot-wire traverse system and the particle image velocimetry system. The up-pointing and down-pointing triangles denote the common flow up and down regions.

Cases	Λ (mm)	z_{VG} (mm)	L_{VG} (mm)
△, ▽	216	14	75
▲, ▼	144	14	75
△, ▽	72	8	18

Table 1: Summary of MVG parameters used in present study.

that are positioned immediately downstream of the SP40 trip. The parameters for the MVG geometry were chosen such that a measurable boundary layer modification was present in excess of 5 m downstream from the MVG trip. Specifically, the spanwise wavelength (Λ), height (z_{VG}) and length (L_{VG}) in the present work corresponds to 216, 14 and 75 mm, respectively (see figure 1, inset A). Further, in order to understand the influence of these parameters on the modified boundary layer, two more cases are surveyed. The MVG parameters used for the three MVG configurations in the current study are summarised in table 1. We note that for all three cases studied the oncoming boundary layer thickness before the MVG array is 20 mm, and so these are classified as sub-boundary layer vortex generators. Furthermore, as illustrated in figure 1 inset A, the MVGs are configured such that the spacing between the adjacent blades is larger in the common flow up region than the common flow down region (denoted using up-pointing and down-pointing triangles, respectively) with a ratio of approximately 4 : 1, corresponding to the configuration which Shahinfar *et al.* (2013) found to provide the strongest modification (i.e. the largest differences in the mean profile from the unperturbed case) to the boundary layer.

In this paper, x, y and z indicate the streamwise, spanwise and wall-normal directions, respectively. The total streamwise velocity is denoted by $\widetilde{U}$, while U and u correspond to the local temporal mean and fluctuations about that local mean velocity (i.e. $\widetilde{U}(\mathbf{x},t) = U(\mathbf{x}) + u(\mathbf{x},t)$, where $\mathbf{x}$ and t denote the position vector and time).

Results

Figure 2(a) shows the development of U downstream of the MVG array, normalised by the freestream velocity, U_∞. The profiles are ordered vertically with the distance from the trip increasing from top to bottom. The three-dimensionality introduced by the MVG results in non-uniform statistics in the spanwise (y) direction. To examine this non-uniformity, downstream measurements are made at two spanwise locations relative to the MVG array. These represent the two lines of spanwise reflectional symmetry for the blade array (as shown in figure 1, inset A). At these locations, we would expect to see flow away from the wall (▲, △) and flow towards the wall (▼, ▽) due to the vortices generated by the MVG array. The solid and open symbols correspond to the Λ = 144 and 216 mm cases respectively, while the solid line is a reference profile with the SP40 trip (referred to hereafter as the canonical case).

From figure 2(a), it is evident that for both cases, the MVG array has introduced spanwise variations in the mean velocity profiles. Higher mean velocities and a reduction in the local boundary layer thickness (red symbols) are observed where the MVG induced counter-rotating vortices produce flow towards the wall. On the other hand, when the flow is directed away from the wall (blue symbols), a reduction in velocity and a thicker local layer thickness is present. Interestingly, for the largest wavelength case (Λ = 216 mm) the modification persists beyond $x > 13$ m or $O(10^3)$ MVG heights, while the study by Marusic *et al.* (2015) indicated that by $O(10^3)$ characteristic height (diameter of the thread rod trip) downstream of a spanwise homogeneous trip, the boundary layer had recovered to the canonical state. Furthermore, since the form drag associated with the MVG trip is smaller than the threaded rod trip, the results suggest that a spanwise heterogeneous disturbance is more efficient at modifying a turbulent boundary layer development compared to a spanwise homogeneous counterpart.

To investigate the strength of the imposed three-dimensionality as a function of x, figure 2(b) shows the integrated difference in the velocity profiles, $\mathcal{U}_d$. Here, $\mathcal{U}_d$ is defined as

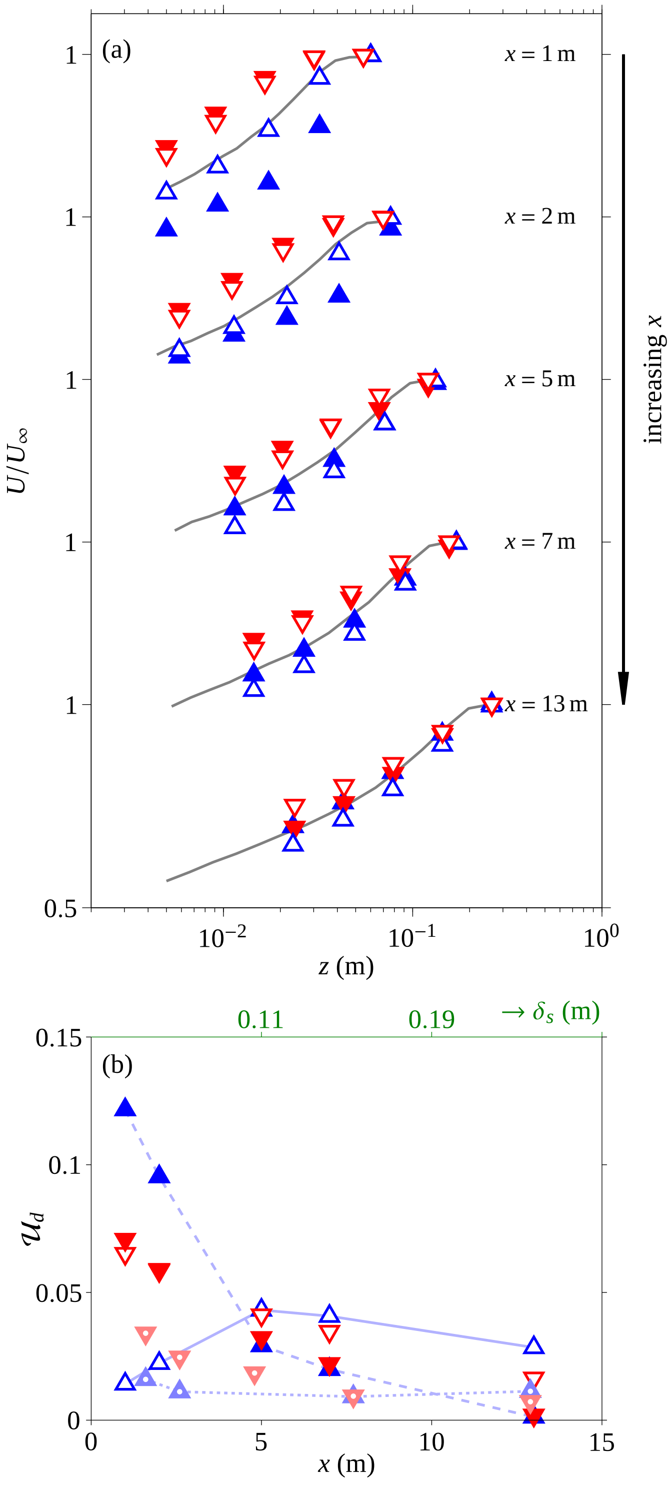

Figure 2: Evolution of the mean velocity profile for the modified and canonical boundary layers. (a) U vs. z (b) $\mathcal{U}_d$ vs. x. The symbols correspond to velocity profiles in the common flow up (△, ▲, △) and down (▽, ▼, ▽) regions; with dotted, solid and open symbols indicating $\Lambda = 72$, 144 and 216 mm cases respectively. Further, the solid line in (a) denotes the canonical profile.

$$\mathcal{U}_d(x) = \left| \int_0^\infty (U - U_s)/U_\infty \, \mathrm{d}\eta \right|,$$

where $U - U_s$ is the difference in the mean velocity between the MVG and the canonical case, while $\eta = z/\delta_s$ where δ_s corresponds to δ of the canonical case. Hence, $\mathcal{U}_d$ provides a measure of the strength of the deviation from the canonical evolution (as a function of development length x) due to the spanwise three-dimensionality introduced by the MVG array. An additional case, corresponding to $\Lambda = 72$ mm case (dotted symbols), based on the optimal parameters from the study of Shahinfar *et al.* (2013), is also included in figure 2(b).

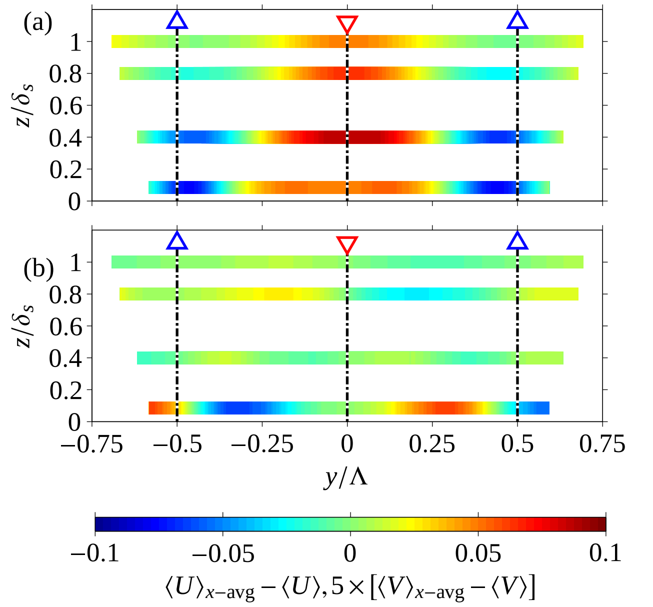

Figure 3: Spanwise variation in the local mean observed for the modified boundary layer using MVG trip. Variation in the streamwise-averaged mean (denoted by $\langle\rangle_{x\text{-avg}}$) corresponding to (a) streamwise and (b) spanwise velocities about their respective global mean (denoted by $\langle\rangle$). Note that for the spanwise velocity, the range of colour contours have been multiplied by 5 to enhance the differences, while symbols △ and ▽ denote the common flow up and down regions, respectively.

Figure 2(b) indicates some interesting differences in the downstream development of the spanwise modes for the three different MVG wavelengths. The $\Lambda = 72$ and 144 mm cases exhibit a monotonic decay in $\mathcal{U}_d$ for both spanwise locations, with all signs of spanwise variation ceasing by $x = 13$ m downstream of the array. Meanwhile, the $\Lambda = 216$ mm case exhibits a more complicated behaviour, with a spanwise variation that persists beyond $x = 13$ m, and $\mathcal{U}_d$ is no longer monotonically decaying with x. Instead, $\mathcal{U}_d$ strengthens up to $x \approx 5$ m, before exhibiting a more gradual decay thereafter. Since the only difference between the $\Lambda = 144$ and 216 mm cases is the spanwise wavelength of the MVG array, this peculiar behaviour highlights that certain spanwise wavelengths tend to be more persistent in the developing layer. The upper abscissa of figure 2(b) shows the boundary layer thickness as a function of x for the canonical case, with the strengthening for the largest wavelength case seeming to coincide with $\Lambda \approx 2\delta$. However at this stage, there still remain unresolved questions regarding the effect of the growth and mutual induction of the counter-rotating vortices generated by the MVG array, which may explain the initial increase in $\mathcal{U}_d$ with x for the $\Lambda = 216$ mm case observed in figure 2.

In order to capture the full spanwise variation of the modified boundary layer, wall-parallel PIV measurements were acquired at approximately 5 m (or 350 MVG heights) from the trip for $\Lambda = 216$ mm case (i.e. where the maximum $\mathcal{U}_d$ is observed). The PIV measurements were performed at four z locations: the geometric mean of the log region ($z^+ = 0.6(\delta^+)^{3/4} \approx 215$), 0.4δ, 0.8δ and δ. Figures 3(a) and (b) show the variation in the streamwise-averaged local mean streamwise ($\langle U\rangle_{x\text{-avg}}$) and spanwise ($\langle V\rangle_{x\text{-avg}}$) velocities

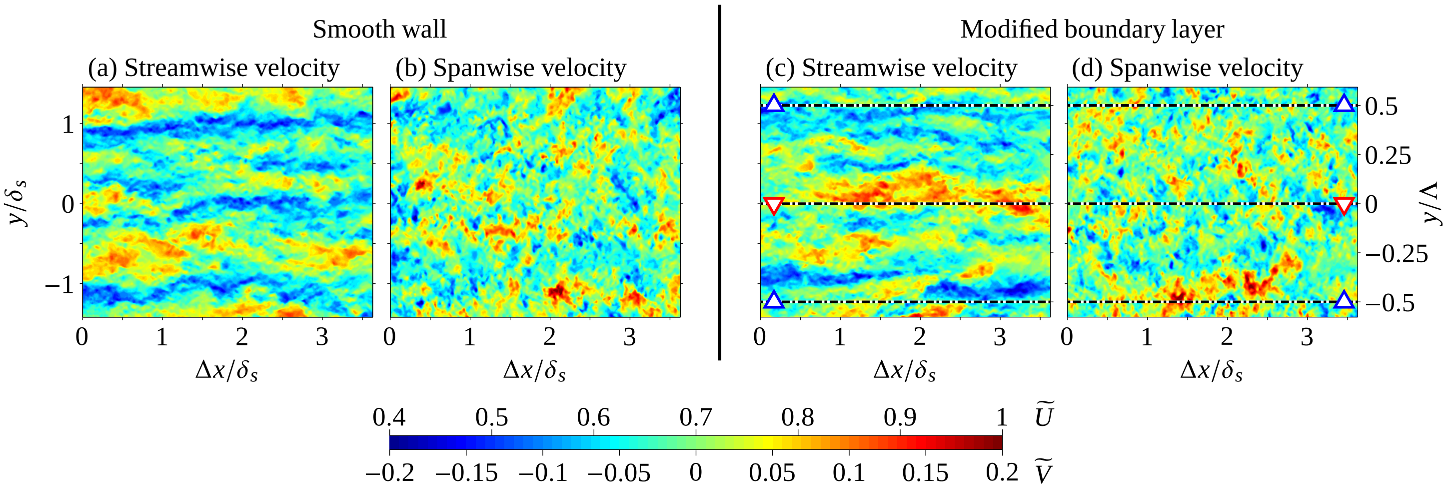

Figure 4: Instantaneous streamwise ($\widetilde{U}$) and spanwise ($\widetilde{V}$) velocities at the geometric mean of the log region ($z^+ = 0.6(\delta^+)^{3/4}$), for the (a,b) canonical boundary layer and (c,d) modified boundary layer using MVG trip. In (c) and (d) symbols △ and ▽ denote the common flow up and down regions, respectively.

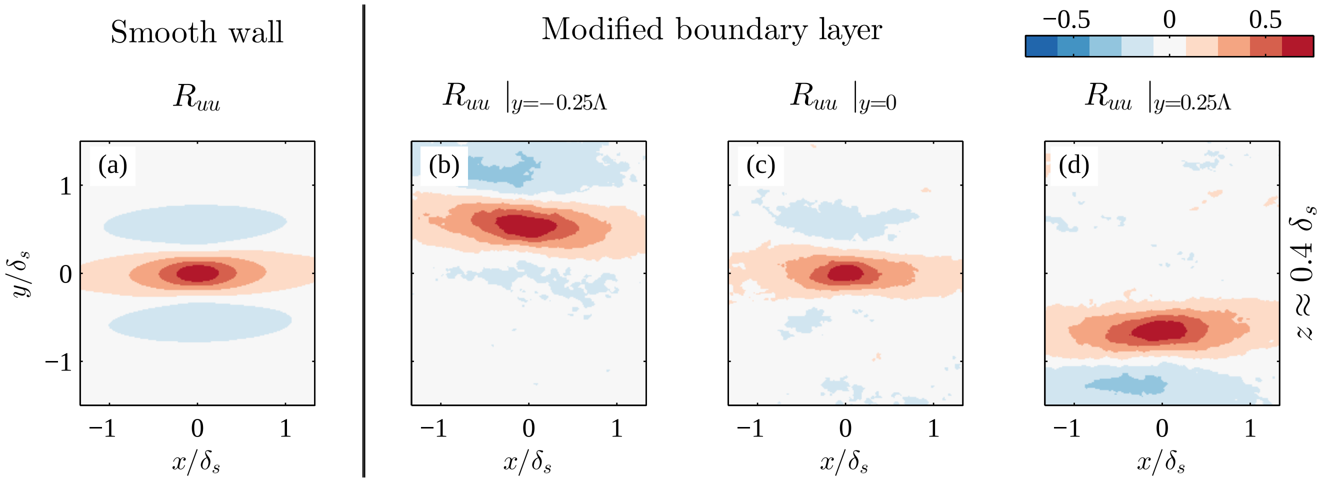

Figure 5: Wall-parallel planes of the normalised two-point correlation for the streamwise velocity (R_{uu}) for the (a) canonical boundary layer and (b-d) modified boundary layer using MVG trip. Results are presented at a wall-normal height of $z \approx 0.4\delta_s$. (b-d) correspond to spanwise locations $y/\Lambda = -0.25, 0$ and 0.25, respectively.

about their respective global mean $\langle U \rangle$ and $\langle V \rangle$, at these heights. It is evident that the counter-rotating roll-modes generated by the MVG trip have lead to a δ-scaled spanwise variation in U and V across the entire wall-normal extent within the boundary layer, which can persist up to ~ 350 MVG heights downstream of the trip. Figures 4(a-d) present an instantaneous velocity field obtained for the canonical and modified turbulent boundary layers at the geometric mean of the log region ($z^+ = 0.6(\delta^+)^{3/4}$). It is evident that the spanwise variation in the local mean for the modified boundary layer (cf. figures 3a and b) is due to preferential alignment of low- and high-speed regions, whereas in the canonical boundary layer they occur in a random arrangement which results in spanwise homogeneity in the mean sense. We note that a similar rearrangement of the low- and high-speed regions also occurs in certain rough wall flows (e.g. converging/diverging riblets, Kevin *et al.*, 2014) where a large-scale counter rotating roll-mode exists.

Figure 5 shows the normalised two-point correlation function for the streamwise velocity (R_{uu}) for the canonical and modified boundary layers at $z/\delta_s \approx 0.4$. Here, the velocity fluctuations are computed relative to the local mean due to the spanwise inhomogeneity for the modified turbulent boundary layer (Coceal & Belcher, 2004). The results show that the flow modification introduced by the MVGs have introduced coherent regions of u that are pronouncedly yawed between the common flow up and down regions. This indicates that in addition to preferentially arranging the large scale structures, the spanwise heterogeneity introduced by the MVG trip has lead to an asymmetry in the δ-scaled u coherence. As these large-scale structures (Hutchins & Marusic, 2007; Kim & Adrian, 1999) are know to carry most of the turbulent energy of the flow (Smits *et al.*, 2011), the results suggest MVGs are capable of modifying these δ-scaled structures and consequently impart a significant influence on the flow. The tilting or meandering of these modes are typically associated with a streak instability mechanism, and the prospect here is that tripping perturbations may be able to interfere with these processes (Flores & Jiménez, 2010).

Modelling the three-dimensional boundary layer evolution

For the spanwise homogeneous disturbances, Perry *et al.* (1994) and Marusic *et al.* (2015) have shown that the subsequent evolution can be predicted with a good accuracy by considering the integrated momentum equation. However, spanwise heterogeneity

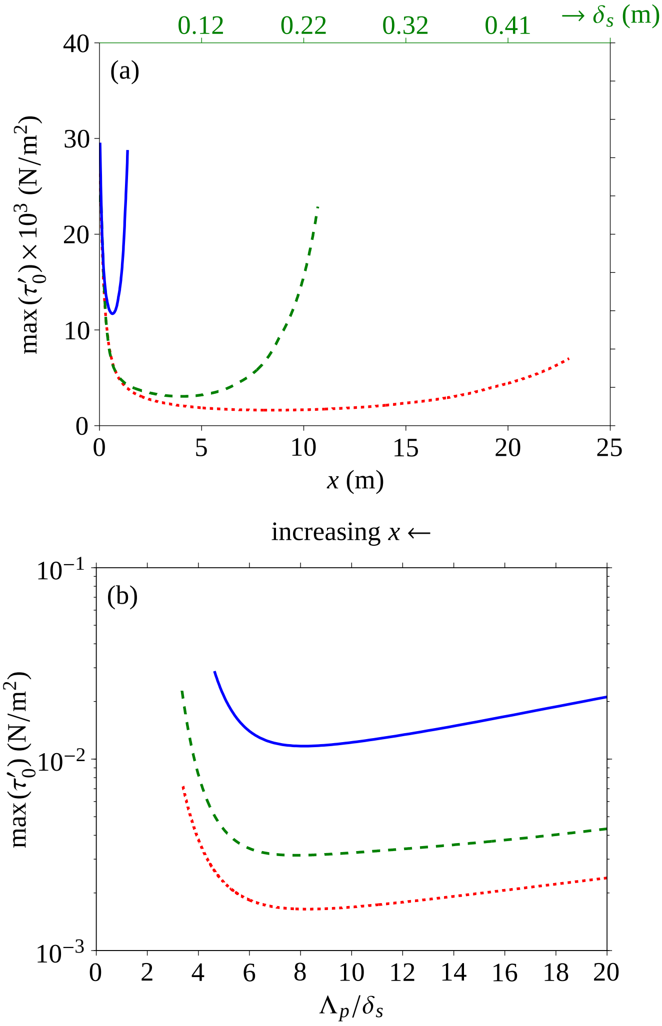

Figure 6: The propagation of disturbances observed for different spanwise wavlength, Λ_p. The variation in the maximum deviation in wall shear stress from the spanwise-averaged value is shown as functions of (a) streamwise development and (b) wavelength as fraction of local boundary layer thickness for the canonical case (δ_s). —— $\Lambda_p = 0.2$ m, - - $\Lambda_p = 0.8$ m and $\cdots$ $\Lambda_p = 1.6$ m.

in the developing layer is not accounted for in the analysis of Perry *et al.* (1994), and here we examine whether by considering the missing term, we can reproduce some of the behaviour observed in the experiment.

Following the balance of forces in the streamwise momentum equation (ignoring the contributions from turbulent stress terms), and integrating from the wall to the freestream region while allowing for lateral variations in U and V, we obtain

$$\frac{\partial}{\partial x}\int_0^\infty U(U-U_\infty)\,\mathrm{d}z + \underbrace{\frac{\partial}{\partial y}\int_0^\infty V(U-U_\infty)\,\mathrm{d}z}_{\text{an additional contribution due to three dimensionality}} = -\frac{\tau_0}{\rho}, \quad (1)$$

where, τ_0 and ρ denote the mean wall shear stress and density, respectively. It should be noted that, here τ_0 is a temporal mean of instantaneous wall shear stress and hence is still a function of x and y. Further, the term containing $\partial/\partial y$ corresponds to an additional contribution due to the presence of spanwise heterogeneity.

Here we will follow the approach taken by Townsend (1976), where a small perturbation restricted to a single spanwise Fourier mode with wavelength Λ_p is considered. Hence

$$\tau_0'\big|_{x=0} = \epsilon\cos\left(\frac{2\pi}{\Lambda_p}y\right), \quad (2)$$

where, $\tau_0' = \tau_0(y) - \frac{1}{\Lambda_p}\int_0^{\Lambda_p}\tau_0(y)\,\mathrm{d}y$ and $\epsilon \ll \frac{1}{\Lambda_p}\int_0^{\Lambda_p}\tau_0(y)\,\mathrm{d}y$. Furthermore, the streamwise mean velocity is assumed to follow a logarithmic profile of the form

$$U = \left(\frac{\tau_0}{\rho}\right)^{\frac{1}{2}}\frac{1}{\kappa}\ln\frac{z}{z_0},\ z < \delta; \quad (3)$$

where $\kappa = 0.39$ is the the von Kármán constant and z_0 corresponds to the wall-normal length scale associated with the roughness (for a smooth wall $z_0 = \mathrm{e}^{-A}(\nu\sqrt{\rho})/\sqrt{\tau_0}$, where $A = 4.3$ corresponds to the intercept of the log law) (Marusic *et al.*, 2013), while the spanwise mean velocity is assumed to obey

$$\frac{\partial V}{\partial z} = \frac{\overline{vw}}{\overline{uw}}\frac{\partial U}{\partial z}. \quad (4)$$

Here, the turbulent stresses $\overline{vw}$ and $\overline{uw}$ are functions of y/Λ_p, z/δ and τ_0 (the readers are referred to Townsend (1976) for the full expressions, which are omitted here for brevity). These assumptions mean that once the initial condition $\tau_0|_{x=0}$ is set, $U|_{x=0}$ and $V|_{x=0}$ are fully defined, and hence $U|_{x=\delta x}$, when δx is small, can be evaluated using (1). This process is repeated to propagate the disturbance τ_0' in x until the final x location is reached.

Figures 6(a) shows how the disturbance τ_0' propagates downstream for different Λ_p as a function of x. The upper axis shows the approximate local boundary layer thickness δ_s. For all three Λ_p cases, the disturbances initially decay. However, after a certain streamwise distance the system becomes unstable and the disturbances are observed to grow in an unbounded manner. This point of growth varies for each wavelength Λ_p considered, with larger wavelengths experiencing growth at a larger x. The unbounded growth in max(τ_0') is unrealistic, and this is because we have neglected the contribution from the turbulent stress terms in (1), which are known to be responsible for the transfer of kinetic energy from the mean to the fluctuating velocities (Tennekes & Lumley, 1972). However, the onset of the growth is interesting. Figure 6(b) shows the development of the disturbance as a function of Λ_p/δ_s, and in this case the minima in max(τ_0') (marking the change from decay to growth) are all well-aligned. Hence this analysis, as originally proposed by Townsend (1976), demonstrates that the x location where the growth of spanwise modes occurs is Λ_p dependent. Furthermore, figure 6(b) suggests that max(τ_0') is minimum when the local boundary layer thickness is approximately 1/8$^{\text{th}}$ of Λ_p, which is consistent with the boundary layer displaying lateral instability for spanwise modes of order δ.

Summary and conclusions

The present work investigates how spanwise periodic modes evolve in a developing zero pressure gradient turbulent boundary layer from their introduction at the trip to downstream locations in excess of 50 characteristic wavelengths. This is achieved by placing an array of miniature (sub-boundary layer) vortex generators at the trip. We find that the spanwise wavelength between a pair of vortex generators plays a critical role in determining the downstream development, and for certain cases, the three-dimensional disturbances can persist for an extended streamwise distance compared to the two-dimensional counterpart. Further, we present preliminary evidence which may support the theoretical prediction by Townsend (1976) that the boundary layer selectively amplifies and sustains lateral variations of $O(\delta)$. In addition to modifying the mean flow, we show that the spanwise disturbances introduced at the trip are also capable of modifying δ-scaled structures that contribute to velocity fluctuations and carry a large portion of the turbulent energy present in the flow. These findings collectively suggest that spanwise heterogeneous perturbation introduced at the trip may be a viable approach to modifying the evolution of developing turbulent boundary layers over a large streamwise development length.

REFERENCES

Baars, W. J., Squire, D. T., Talluru, K. M., Abbassi, M. R., Hutchins, N. & Marusic, I. 2016 Wall-drag measurements of smooth-and rough-wall turbulent boundary layers using a floating element. *Exp. Fluids* **57** (5), 1–16.

Bradshaw, P. 1965 The effect of wind-tunnel screens on nominally two-dimensional boundary layers. *J. Fluid Mech.* **22** (04), 679–687.

Castillo, L. & Johansson, T. G. 2002 The effects of the upstream conditions on a low Reynolds number turbulent boundary layer with zero pressure gradient. *J. Turbul.* **3** (31), 1–19.

Coceal, O. & Belcher, S. E. 2004 A canopy model of mean winds through urban areas. *Q. J. R. Meteorolog. Soc.* **130** (599), 1349–1372.

Flores, O. & Jiménez, J. 2010 Hierarchy of minimal flow units in the logarithmic layer. *Phys. Fluids* **22** (7), 071704.

Furuya, Y., Nakamura, I. & Osaka, H. 1979 Three-dimensional structure of a nominally planar turbulent boundary layer. *J. Fluid Eng.* **101**, 326–230.

Gong, W., Taylor, P. A. & Dörnbrack, A. 1996 Turbulent boundary-layer flow over fixed aerodynamically rough two-dimensional sinusoidal waves. *J. Fluid Mech.* **312**, 1–37.

Hutchins, N. & Marusic, I. 2007 Evidence of very long meandering features in the logarithmic region of turbulent boundary layers. *J. Fluid Mech.* **579**, 1–28.

Kevin, Nugroho, B., Monty, J. P. & Hutchins, N. 2014 Wall-parallel PIV measurements in turbulent boundary layers with highly directional surface roughness. In *Proc. 19th Australas. Fluid Mech. Conf.*.

Kim, K. C. & Adrian, R. J. 1999 Very large-scale motion in the outer layer. *Phys. Fluids* **11** (2), 417–422.

Klebanoff, P. S. & Tidstrom, K. D. 1959 Evolution of amplified waves leading to transition in a boundary layer with zero pressure gradient. *Tech. Rep.* NASA-TN-D195. NASA.

Marusic, I., Chauhan, K. A., Kulandaivelu, V. & Hutchins, N. 2015 Evolution of zero-pressure-gradient boundary layers from different tripping conditions. *J. Fluid Mech.* **783**, 379–411.

Marusic, I., Monty, J. P., Hultmark, M. & Smits, A. J. 2013 On the logarithmic region in wall turbulence. *J. Fluid Mech.* **716**, 716.

Mejia-Alvarez, R. & Christensen, K. T. 2013 Wall-parallel stereo particle-image velocimetry measurements in the roughness sublayer of turbulent flow overlying highly irregular roughness. *Phys. Fluids* **25** (11), 115109.

Nickels, T. B., Marusic, I., Hafez, S. & Chong, M. S. 2005 Evidence of the k_1^{-1} law in a high-Reynolds-number turbulent boundary layer. *Phys. Rev. Lett.* **95** (7), 074501.

Perry, A. E., Marusic, I. & Li, J. D. 1994 Wall turbulence closure based on classical similarity laws and the attached eddy hypothesis. *Phys. Fluids* **6** (2), 1024–1035.

Pook, D. A., Watmuff, J. H. & Orifici, A. C. 2016 Test section streaks originating from imperfections in a zither located upstream of a contraction. *J. Fluid Mech.* **787**, 254–291.

Reynolds, R. T., Hayden, P., Castro, I. P. & Robins, A. G. 2007 Spanwise variations in nominally two-dimensional rough-wall boundary layers. *Exp. Fluids* **42** (2), 311–320.

Schlatter, P. & Örlü, R. 2011 Turbulent boundary layers at moderate Reynolds numbers: inflow length and tripping effects. *J. Fluid Mech.* **710**, 5–34.

Shahinfar, S., Fransson, J. M., Sattarzadeh, S. S. & Talamelli, A. 2013 Scaling of streamwise boundary layer streaks and their ability to reduce skin-friction drag. *J. Fluid Mech.* **733**, 1–32.

Smits, A. J., McKeon, B. J. & Marusic, I. 2011 High-Reynolds number wall turbulence. *Annu. Rev. Fluid Mech.* **43**, 353–375.

Tennekes, H. & Lumley, J. L. 1972 *A first course in turbulence*. MIT Press.

Townsend, A. A. 1976 *The structure of turbulent shear flow*, 2nd edn. Cambridge Univ Press.

Watmuff, J. H. 1998 Detrimental effects of almost immeasurably small freestream nonuniformities generated by wind-tunnel screens. *AIAA Journal* **36** (3), 379–386.